Hard X-Ray Phase Tomography with Low-Brilliance Sources

F. Pfeiffer, C. Kottler, O. Bunk, and C. David
Paul Scherrer Institut, CH-5232 Villigen PSI, Switzerland
(Received 10 November 2006; published 8 March 2007)

We report on a method for tomographic phase contrast imaging of centimeter sized objects. As opposed to existing techniques, our approach can be used with low-brilliance, lab based x-ray sources and thus is of interest for a wide range of applications in medicine, biology, and nondestructive testing. The work is based on the recent development of a hard x-ray grating interferometer, which has been demonstrated to yield differential phase contrast projection images. Here we particularly focus on how this method can be used for tomographic reconstructions using filtered back projection algorithms to yield quantitative volumetric information of both the real and imaginary part of the samples's refractive index.

DOI: 10.1103/PhysRevLett.98.108105 PACS numbers: 87.59.Hp, 07.85.Fv, 87.59.Fm

Phase-sensitive x-ray imaging, which uses the phase shift rather than the absorption as the imaging signal, has the potential of substantially increased contrast in biological samples [1–3]. Various phase-sensitive x-ray imaging methods were developed in the past years. They can be classified into interferometric methods [4–9], techniques using an analyzer crystal [10–12], and free-space propagation methods [13–16]. Some of them have been extended to three-dimensional (3D) x-ray phase computed tomography (CT) and yield excellent results, when highly brilliant synchrotron radiation is used.

It has recently been demonstrated that laboratory based x-ray phase CT is in principle possible and can yield excellent results for microscopic samples [17,18]. However, several constraints impair the application of the existing approaches as a standard method in hospital based medical imaging. One of the most severe limitations is that the methods require sufficiently brilliant radiation, which is presently only available from sources with small enough source dimensions (typically a few microns) and correspondingly low-power (a few Watts). The limited field of view, the in-vacuum setup, and the homogeneous object [19] or pure phase object [20] approximation for the phase retrieval algorithm further restrict the existing techniques to specific micro-CT studies [18]. This is why x-ray phase tomography, despite of its potential for improved contrast, is currently not available as a standard 3D characterization tool for medical, biological or industrial applications.

Here we report how an alternative approach using a hard x-ray grating interferometer can be used for quantitative CT phase reconstructions of macroscopic, centimeter sized objects with standard x-ray tube sources with square millimeter source dimensions and correspondingly high power (> 1 kW). The work is based on the recent development of a hard x-ray grating interferometer, which has been demonstrated to yield two-dimensional (2D) differential phase contrast (DPC) projection images [21]. In this article we particularly focus on how the latter 2D method can be extended into 3D with an adapted filtered back projection reconstruction algorithm to yield quantitative volumetric information of both the real and imaginary part of the refractive index.

CT algorithms for reconstructing an object, $g(x, y)$, from its projections (Radon transform),

$$\mathcal{G}(y', \omega) = \int_{-\infty}^{\infty} g(x', y')dx', \tag{1}$$

are well known (see Fig. 1 and [22,23]). A fast and accurate algorithm is filtered back projection (FBP). It can be represented by the convolution back projection integral [22,24]

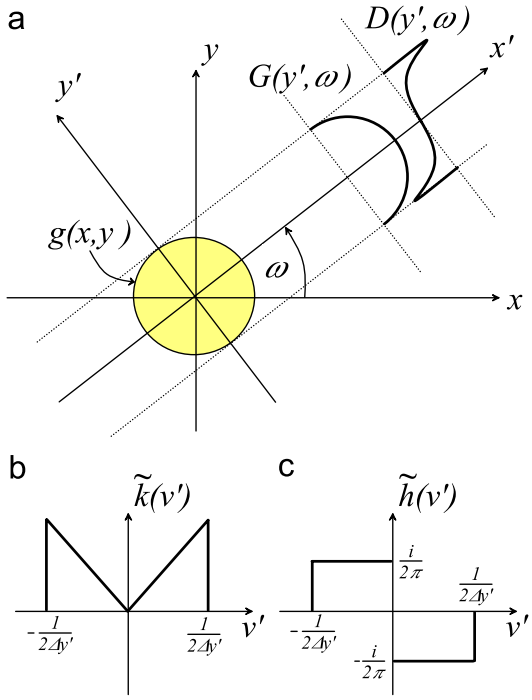

FIG. 1 (color online). Tomographic reconstruction. (a) Projection geometry. (b),(c) Back projection filter functions for (b) simple projection line integrals and (c) gradient projection integrals.

$$g(x, y) = \int_0^{\pi} \mathcal{FT}^{-1}[\tilde{\mathcal{G}}(v', \omega)\tilde{k}(v')]d\omega, \qquad (2)$$

where $\tilde{\mathcal{G}}(v', \omega)$ is the Fourier transform of $\mathcal{G}(y', \omega)$, v' (y') is the reciprocal (real) space coordinate corresponding to a coordinate system rotated by an angle ω around the tomographic rotation axis, $\tilde{k}(v')$ is the Fourier representation of the filter function, and $\mathcal{FT}^{-1}$ denotes an inverse Fourier transform. In the case of simple line projections, e.g., for absorption based tomography, the filter is defined as $\tilde{k}(v') \equiv |v'|$ [see Fig. 1(b) and [25]].

In our case, however, the experimental arrangement not only yields the line projection of the object function [Eq. (1)], but also the line projections of the partial derivative of the object function:

$$\mathcal{D}(y', \omega) = \int_{-\infty}^{\infty} \frac{\partial g(x', y')}{\partial y'} dx'. \qquad (3)$$

In this case tomographic reconstruction based on the conventional FBP using the standard linear filter function [Fig. 1(b)] will not result in a correct reconstruction of the original object function. As has been suggested by Faris *et al.* [26] in the case of visible light tomography, the problem can be solved by adapting the filter function in the FBP algorithm accordingly. More precisely the object can again be expressed in the form of a convolution back projection integral,

$$g(x, y) = \int_0^{\pi} \mathcal{FT}^{-1}[\tilde{\mathcal{D}}(v', \omega)\tilde{h}(v')]\, d\omega, \qquad (4)$$

provided that in this case an imaginary filter function $\tilde{h}(v') \equiv 1/2\pi i \mathrm{sgn}(v')$ is used, where $\mathrm{sgn}(v')$ is the sign function [Fig. 1(c)]. Note that this type of filtering corresponds to a Hilbert transform in real space.

In practice our DPC imaging setup consists of a source grating G0, a phase grating G1, and an analyzer absorption grating G2 [Fig. 2(a)]. The source grating (G0), typically placed close to the x-ray tube anode, is an arrayed aperture mask with transmitting slits. It effectively allows for the use of relatively large, i.e., square millimeter sized x-ray sources, without compromising on the coherence requirements of the DPC method [21,27]. The DPC itself is formed within the two gratings G1 and G2 and is similar to Schlieren imaging [28] or diffraction-enhanced imaging [10,12]. It essentially relies on the fact that a phase object placed in the x-ray beam path causes a slight deflection of the beam transmitted through the object [Fig. 2(b)]. The fundamental idea of DPC imaging depends on locally detecting these angular deviations. The angle is directly proportional to the local gradient of the object's phase shift $\Phi(y, z)$ and can be quantified by [28]

$$\alpha(y, z) = \frac{\lambda}{2\pi} \frac{\partial \Phi(y, z)}{\partial y} = \int_{-\infty}^{\infty} \frac{\partial \delta(x, y, z)}{\partial y} dx, \qquad (5)$$

where λ is the wavelength of the x rays and $\delta(x, y, z)$ the

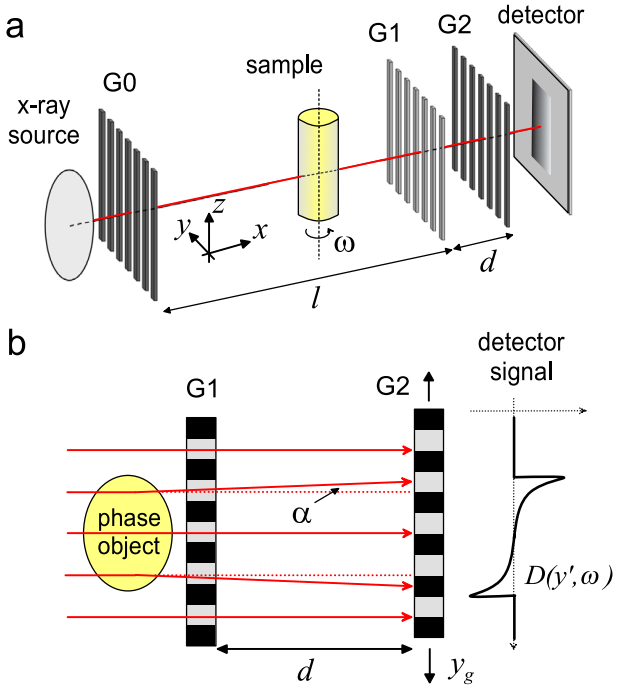

FIG. 2 (color online). X-ray imaging interferometer. (a) Setup based on transmission gratings G0 through G2. (b) A phase object in the beam path causes a slight deflection of x rays changing the locally transmitted intensity through the arrangement formed by the gratings G1 and G2.

decrement of the real part of the object's refractive index $n(x, y, z)$. As described in more detail in [29], a set of images taken for different positions of the grating G2 (phase-stepping scan) can be used to simultaneously obtain both the DPC images and the conventional transmission projections $\exp[-\int_{-\infty}^{\infty} 4\pi\beta(x, y, z)/\lambda\, dx]$, where $\beta(x, y, z)$ is the imaginary part of the objects refractive index distribution. The so obtained DPC and transmission projections can directly be used as input for the two FBP algorithms previously described in Eqs. (2) and (4), respectively.

The experiments were carried out on a Seifert ID 3000 x-ray generator operated at 35 kV/30 mA. We used a tungsten (W) line focus tube (DX-W8 × 0.4-L) with a focus size of 8 (hor) × 0.4 (ver) mm^2. Because of the inclination of the target with respect to the optical axis of our setup of 6°, the effective source size was 0.8 (hor) × 0.4 (ver) mm^2. The gratings were fabricated by a process involving photolithography, deep etching into silicon, and electroplating of gold. They were placed with their lines perpendicular to the optical axis of the setup and parallel to the axis of tomographic rotation [30]. The images were recorded using a 150 micron thick cesium iodide (CsI) scintillation screen with a demagnifying optical lens system and a cooled charge coupled device [31,32].

Figures 3(a) and 3(b) show absorption and differential phase contrast projections of a reference sample containing

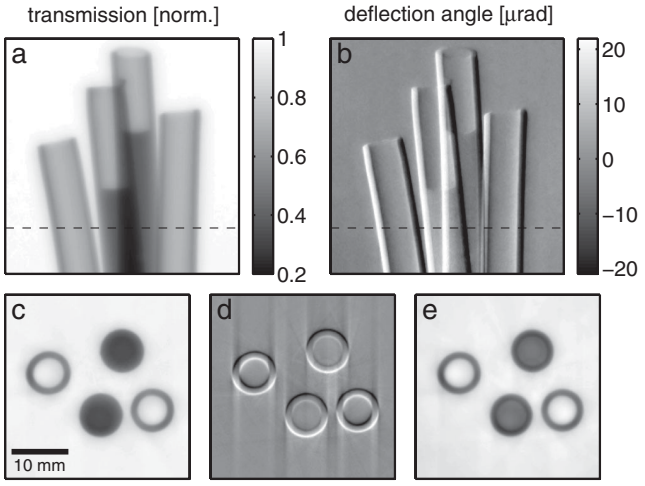

FIG. 3. Results for a test sample containing empty and water-filled Teflon plastic tubes. (a) Conventional x-ray absorption projection; (b) differential phase contrast (DPC) projection; (c)–(e) tomograms obtained from (c) the logarithm of the absorption projections using the linear filter [Fig. 1(b)]; (d) the DPC projections using the linear filter [Fig. 1(b)]; and (e) the DPC projections using the imaginary sign filter [Fig. 1(c)]. The total exposure time for the 360 projections was 2 h.

PTFE (polytetrafluoroethylene) tubes. Two of the four tubes were filled with a saltwater solution. A slice through the reconstructed 3D volume data set of $\beta(x, y, z)$, using the conventional FBP algorithm [Eq. (2)] with the real, linear filter function [Fig. 1(b)] and the logarithm of the transmission projections as an input is shown in Fig. 3(c). If the same algorithm is applied to the DPC projections, the differential nature of the signal is transferred to the tomographic reconstruction. This causes quite strong artifacts in the reconstructed volume [see Fig. 3(d)]. With the DPC-FBP algorithm [Eq. (4)] and the corresponding imaginary filter function [Fig. 1(c)] a correct reconstruction of $\delta(x, y, z)$, from the DPC projections is achieved [Fig. 3(e)]. Note that due to their similar absorption cross sections a differentiation of the plastic from the saltwater liquid is hardly possibly based on the absorption signal [Fig. 3(c)]. The reconstructed distribution of $\delta(x, y, z)$, however, shows a significant contrast between the materials [33].

Figure 4 displays the results of applying our method to a more complex, biological object (a hornet). It shows one DPC projection, a frontal slice through the reconstructed 3D distribution of $\delta(x, y, z)$, and a 3D rendering of the specimen [34]. The results reveal details of the internal structure and clearly demonstrate that DPC-CT is applicable to complex biological objects. This illustrates that our method provides an alternative approach for obtaining 3D x-ray CT information without the explicit necessity of absorbing x rays in the object. A further development of the method towards higher x-ray energies, and correspondingly lower absorption, will potentially provide a significant dose reduction. This is not possible for conventional absorption based CT methods, where a lower absorption in the object inevitably results in a corresponding loss of image contrast.

In conclusion, we have shown how a setup consisting of three transmission gratings together with appropriate tomographic FBP algorithms can yield quantitative 3D information of the real and imaginary part of the refractive index distribution of macroscopic objects. In contrast to existing techniques [17,18] our approach can be used with conventional x-ray tube sources with square millimeter source sizes and several kW power. It is significantly more efficient, not restricted to homogeneous objects [19] or weakly absorbing objects [20], and does not require the sample to be in vacuum.

We have demonstrated the capabilities by presenting full three-dimensional tomographic phase and absorption reconstructions of centimeter sized test samples and more complex biological objects. Based on these results we

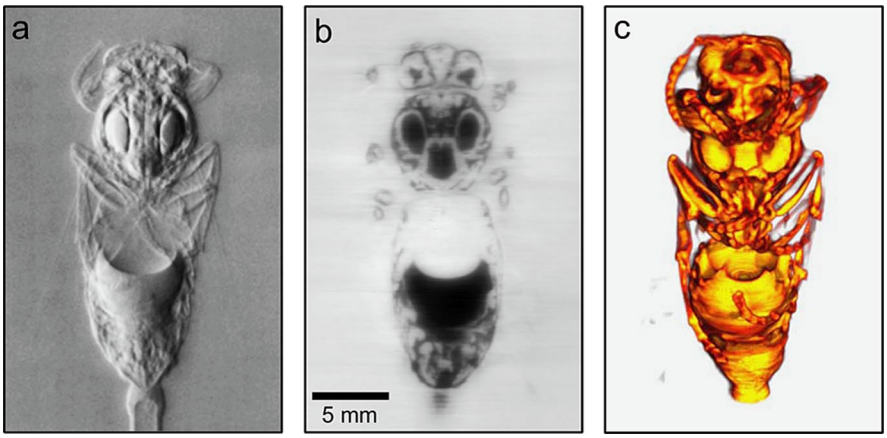

FIG. 4 (color online). Results for a biological object (a hornet). (a) Differential phase contrast projection; (b) tomographic slice through the reconstructed distribution of the real part of the refractive index $\delta(x, y, z)$; and (c) 3D rendering of $\delta(x, y, z)$ (see also [34]). The volume data set of $400 \times 400 \times 800$ voxels was reconstructed from 360 projections recorded within a total exposure time 6 h [35].

conclude that our method represents a major step forward in x-ray phase tomography with lab based x-ray sources that provides all of the information imparted by conventional x-ray CT, with the potential of yielding additional and complementary information through the phase contrast signal. Thus we envision a widespread application of our method in areas where x-ray phase tomography would be desirable, but is currently unavailable. For example, we believe that this method can readily be implemented without major changes to nondestructive industrial desktop tomography systems, small animal imaging, or biomedical applications. Finally, upon further development of the method for higher x-ray energies, the application in medical x-ray CT scanners can potentially yield an increased soft tissue sensitivity for x-ray CT which presently is only available through much more expensive techniques, like, e.g., magnetoresonance imaging.

C. K. acknowledges support through the KTI under Contract No. 7796.2 DCPP-NM. We gratefully acknowledge the assistance of J. Bruder, C. Grünzweig, and E. Güzel in the experiments and T. Weitkamp, M. Stampanoni, and P. Cloetens for fruitful discussions.

[1] R. Fitzgerald, Phys. Today **53**, No. 7, 23 (2000).
[2] A. Momose, Opt. Express **11**, 2303 (2003).
[3] A. Momose, Jpn. J. Appl. Phys. **44**, 6355 (2005).
[4] U. Bonse and M. Hart, Appl. Phys. Lett. **6**, 155 (1965).
[5] U. Bonse and F. Busch, Prog. Biophys. Molec. Biol. **65**, 133 (1996).
[6] A. Momose, Nucl. Instrum. Methods Phys. Res. **352**, 622 (1995).
[7] A. Momose, T. Takeda, Y. Itai, and K. Hirano, Nature Medicine **2**, 473 (1996).
[8] F. Beckmann, U. Bonse, F. Busch, and O. J. Gunnewig, J. Comput. Assist. Tomogr. **21**, 539 (1997).
[9] F. Beckmann *et al.*, Biophys. J. **76**, 98 (1999).
[10] V. N. Ingal and E. A. Beliaevskaya, J. Phys. D **28**, 2314 (1995).
[11] T. J. Davis, D. Gao, T. E. Gureyev, A. W. Stevenson, and S. W. Wilkins, Nature (London) **373**, 595 (1995).
[12] L. D. Chapman, W. C. Thomlinson, R. E. Johnston, D. Washburn, E. Pisano, N. Gmuer, Z. Zhong, R. Menk, F. Arfelli, and D. Sayers, Phys. Med. Biol. **42**, 2015 (1997).
[13] A. Snigirev, I. Snigireva, V. Kohn, S. Kuznetsov, and I. Schelokov, Rev. Sci. Instrum. **66**, 5486 (1995).
[14] S. W. Wilkins, T. E. Gureyev, D. Gao, A. Pogany, and A. W. Stevenson, Nature (London) **384**, 335 (1996).
[15] K. A. Nugent, T. E. Gureyev, D. F. Cookson, D. Paganin, and Z. Barnea, Phys. Rev. Lett. **77**, 2961 (1996).
[16] P. Cloetens, W. Ludwig, J. Baruchel, D. van Dyck, J. van Landuyt, J. P. Guigay, and M. Schlenker, Appl. Phys. Lett. **75**, 2912 (1999).
[17] S. C. Mayo, P. R. Miller, S. W. Wilkins, T. J. Davis, D. Gao, T. E. Gureyev, D. Paganin, D. J. Parry, A. Pogany, and A. W. Stevenson, J. Microsc. **207**, 79 (2002).
[18] S. C. Mayo, T. J. Davis, T. E. Gureyev, P. R. Miller, D. Paganin, A. Pogany, A. W. Stevenson, and S. W. Wilkins, Opt. Express **11**, 2289 (2003).
[19] D. Paganin, S. C. Mayo, T. E. Gureyev, P. R. Miller, and S. W. Wilkins, J. Microsc. **206**, 33 (2002).
[20] A. V. Bronnikov, Opt. Commun. **171**, 239 (1999).
[21] F. Pfeiffer, T. Weitkamp, O. Bunk, and C. David, Nature Phys. **2**, 258 (2006).
[22] G. T. Herman, *Image Reconstruction from Projections* (Academic Press, New York, 1980).
[23] A. C. Kak and M. Slaney, *Principles of Computerized Tomography* (IEEE Press, New York, 1987).
[24] Note that we have omitted the third dimension (z axis) because it does not affect the further derivation.
[25] In practice, where the projections are sampled with a finite resolution, $\Delta y'$, this filter is truncated at the Nyquist frequency, $\frac{1}{2}\Delta y'$ [see Fig. 1(b) and 1(c)].
[26] G. W. Faris and R. L. Byer, Appl. Opt. **27**, 5202 (1988).
[27] F. Pfeiffer, O. Bunk, T. Weitkamp, J. F. van der Veen, and I. K. Robinson, Phys. Rev. Lett. **94**, 164801 (2005).
[28] M. Born and E. Wolf, *Principles of Optics* (Pergamon Press, Oxford,1980).
[29] T. Weitkamp, A. Diaz, C. David, F. Pfeiffer, M. Stampanoni, P. Cloetens, and E. Ziegler, Opt. Express **13**, 6296 (2005).
[30] They had periods of: $p_0 = 73\ \mu$m, $p_1 = 3.9\ \mu$m, and $p_2 = 2.0\ \mu$m. The height of the grating structures were 42 μm (G0), 35 μm (G1), and 26 μm (G2). The distances between the gratings were $l = 1.57$ m and $d = 43$ mm.
[31] The effective spatial resolution was mainly determined by the thickness of the scintillation screen to ≈ 0.1 mm. The field of view is currently limited by the 100 mm wafer processing technology to 64×64 mm^2. No principle constraints hinder the upscaling by using state-of-the-art (300 mm) techniques.
[32] Fingerlakes Instrumentation, FLI IMG 1001, KODAK chip with 1024×1024 pixels, $24 \times 24\ \mu$m^2 pixel size.
[33] The polytetrafluoroethylene (PTFE) plastic tubes had a density of $\rho_{\mathrm{PTFE}} = 2.2$ g/cm^3 and a radius of $R = 3.0$ mm with a hollow core of $r = 2.0$ mm. The corresponding density value for the saltwater solution (4.4 mol/dm^2 NaCl) was $\rho_{\mathrm{saltwater}} = 1.18$ g/cm^3. From the gray values of the reconstructed tomograms [Fig. 3(e)], we deduce values of $\delta_{\mathrm{PTFE}} \simeq 5.1 \times 10^{-7}$ and $\delta_{\mathrm{saltwater}} \simeq 3.9 \times 10^{-7}$. Assuming a mean energy of $E_{\mathrm{mean}} \simeq 28$ keV this agrees, within $\approx 10\%$, with the tabulated literature values.
[34] See EPAPS Document No. E-PRLTAO-98-008712 for movies containing the measured phase contrast projections, slices through the reconstructed volume, and a 3D animation of the rendered object. For more information on EPAPS, see http://www.aip.org/pubservs/epaps.html.
[35] For one projection, four individual raw images (phase-stepping) with exposure times of 5 (Fig. 3) or 15 (Fig. 4) seconds each were recorded. The total exposure time can be greatly reduced by (a) using a more efficient detector, (b) decreasing the distance between the source and the sample, and (c) using standard rotating anode x-ray generators with a power of several kW.